TRIUMF Beam Physics Note
TRI-BN-16-14
2016/09/01 - 2016/09/03

Investigating 94Sr Tune Loss: ISAC RPM Data Summary

C. Barquest

TRIUMF

Abstract: Between Sep. 1-3, four measurement sets of RPM (Rotational Profile Monitor) data were taken at ISAC using RPMs X/Y3A, X/Y3C, X/Y6A, X/Y6B, 14, 18, and 31 in an attempt to characterize the unexplained drift of 94Sr beams through the ISAC Mass Separator Room. Each scan set observed the 94Sr beam disappear at FC34; stable transmission could never be maintained. A summary of the data from these scan sets is presented, with concluding remarks on possible causes of data trends observed and lessons learned.

4004 Wesbrook Mall, Vancouver, B.C. Canada V6T 2A3 Tel: 604 222-1047 Fax: 604 222-1074
www.triumf.ca

1 Measurement Overview

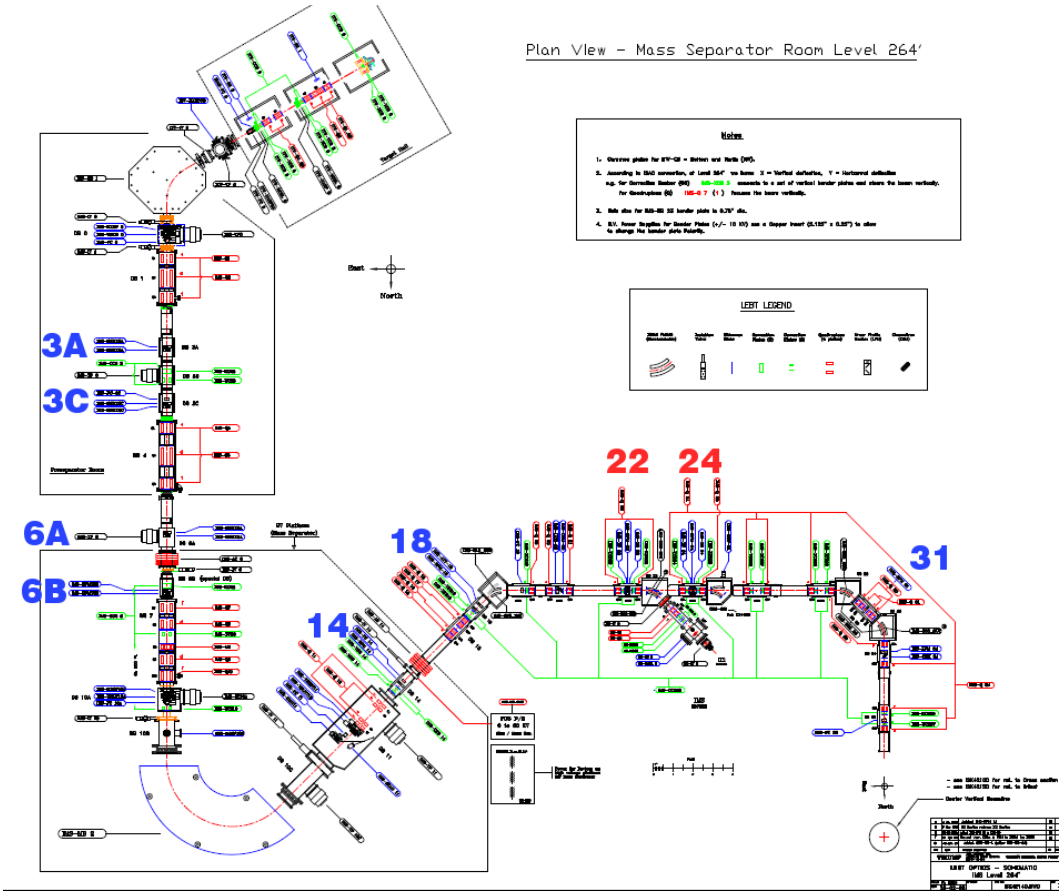

Figure 1: ISAC Mass Seperator Room RPM locations. RPMs indicated in red (22, 24) were inoperable for the duration of these scansets.

The beam's center position and rms size were measured using RPMs at locations shown in Figure 1. For each run, RPM scans were taken at regular intervals to deduce trends in the data over time (note: X=vertical and Y=horizontal to adhere with convention for this beamline).

Data from each scan set is separated into two sets of RPM plots: upstream (3A, 3C, 6A, 6B) and downstream (14, 18, 31) of the bending magnet. Measurements at RPMs 22 and 24 were unavailable at the time of these scans, and it was discovered that data from RPM 18 was also unreliabled (see Figure 6).

The four runs are labeled Run0-3. At RPM31 the longest measurement acheived for 94Sr was two hours. Although Run2 contains no 94Sr RPM data, this run was included in this summary to highlight how quickly the beam can be lost, and that the rate of the 94Sr drift is not constant across runs.

2 Run0: 2016/09/01 2hr: 94Sr @ 12.78kV

2.1 Current Evolution

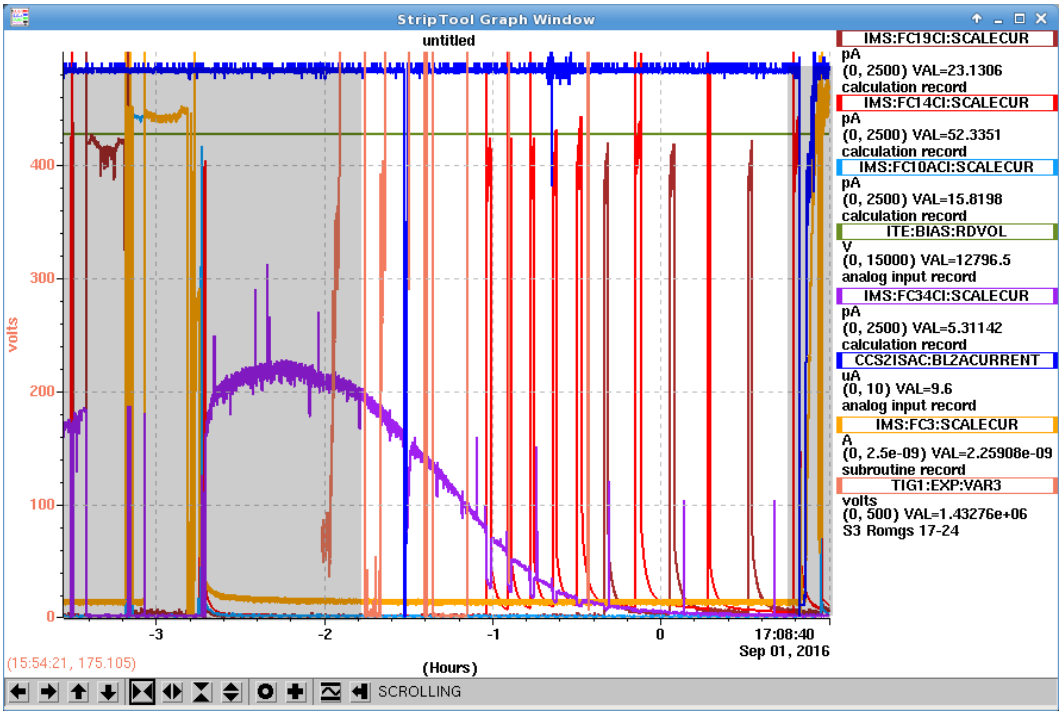

Figure 2: 94Sr FC34 Trend with highlighted Run0 time: 09/01 14:20-16:55.

Run0 is characterized by the loss of 94Sr beam over two hours of run time at FC34 as shown by the purple plot in Figure 2. Beam current is stable at FC14 and FC19 (red and brown plots respectively).

2.2 Beam Position Evolution

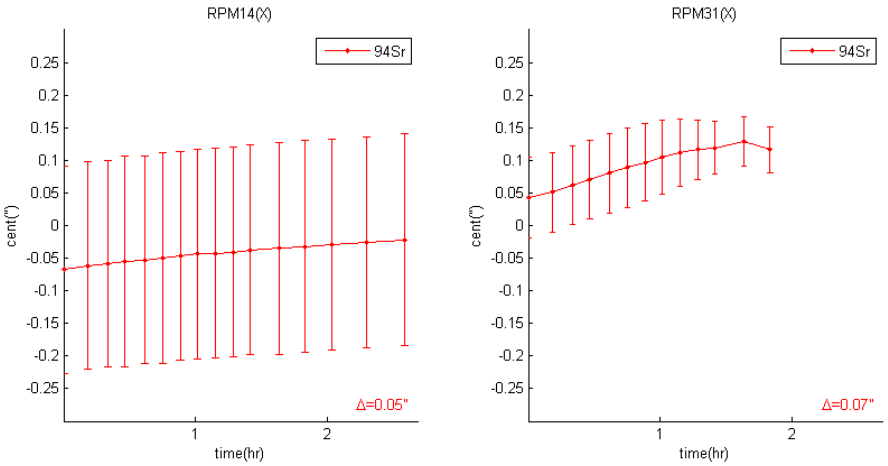

Figure 3: Run0: X_{cen} vs $t_{elapsed}$. Vertical beam at RPM14 and RPM31. Error bars are profile scan RMS beam size, not an indication of measurement precision.

Figure 3 shows a slight shift in the vertical beam position at RPM14 ($\Delta x =$ 0.05" over 2.5hrs) which suggests the origin of the problem lies upstream. The change in vertical beam position at RPM31 ($\Delta x = 0.05$" over 1hr) is large enough that the beam begins to be collimated towards the end of the scan. This can be seen in Figure 3 as the RMS size begins to decrease. The RPM31 profile data for the final three data points of the scan set could not be analyzed to return centroid and rms values, indicating loss of the beam.

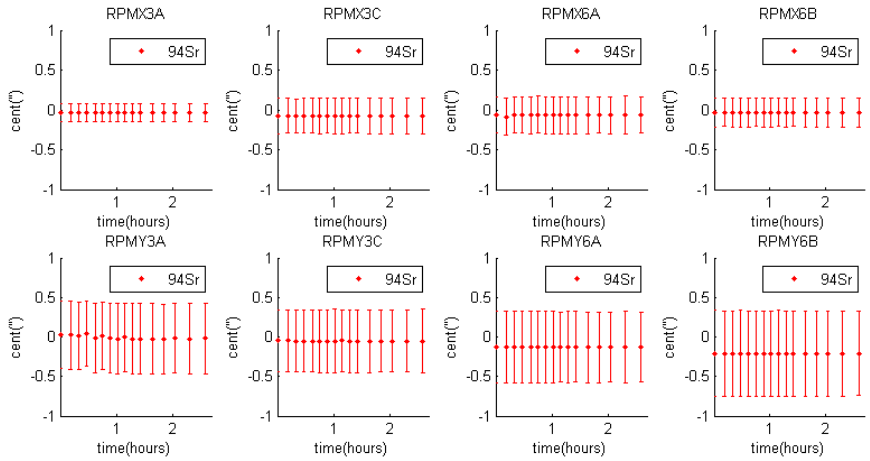

Figure 4: Run0: RPMs: 3A, 3C, 6A, and 6B. X_{cen} vs $t_{elapsed}$ Vertical centroid and rms in first row. Y_{cen} vs $t_{elapsed}$ Horizontal centroid and rms in second row.

Plotting the RPM data for both Y and X in Figure 4 shows a stable beam position from 3A-6B for the entire 2.5hrs of the scan. This implies that the issue occurs downstream of the RPMs at 6B.

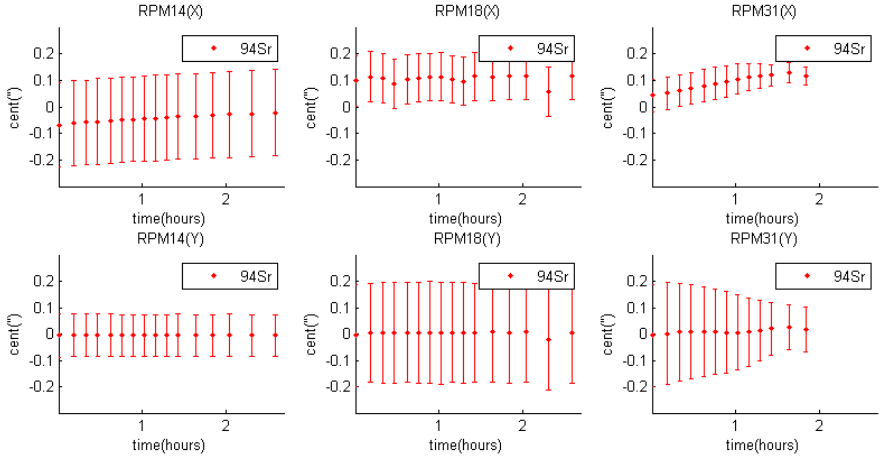

Figure 5: Run0: RPMs: 14, 18, 31. X_{cen} vs $t_{elapsed}$ Vertical centroid and rms in first row. Y_{cen} vs $t_{elapsed}$ Horizontal centroid and rms in second row.

Plotting the RPM data for both Y and X in Figure 5 shows that the horizontal position of the beam appears stable from 14-31 for the entire 2.5hrs of the scan (omitting the last half hour when data is not available at RPM31). The same is not true of the vertical position of the beam as discussed earlier.

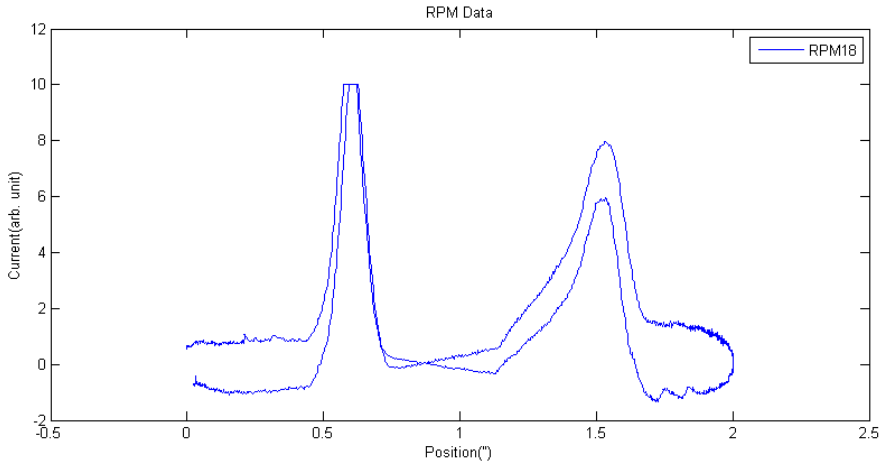

Figure 6: Run0: Current(arb. units) vs Position(") for a scan at RPM18. Note that the first and second half of the scan ("in" and "out") read back different current for the same position, indicating that there is a changing background signal (perhaps induced by the movement of the scanner itself?) This may lead to unreliable position/rms reconstruction.

3 Run1: 2016/09/01-02 5hr 238U → 6hr 94Sr

3.1 Current Evolution

238U current increases then slightly decreases at FC34 over the course of five hours. Switching to 94Sr, the current decreases at FC34 over the course of one hour. Then the beam is monitored at FC19 over the next five hours.

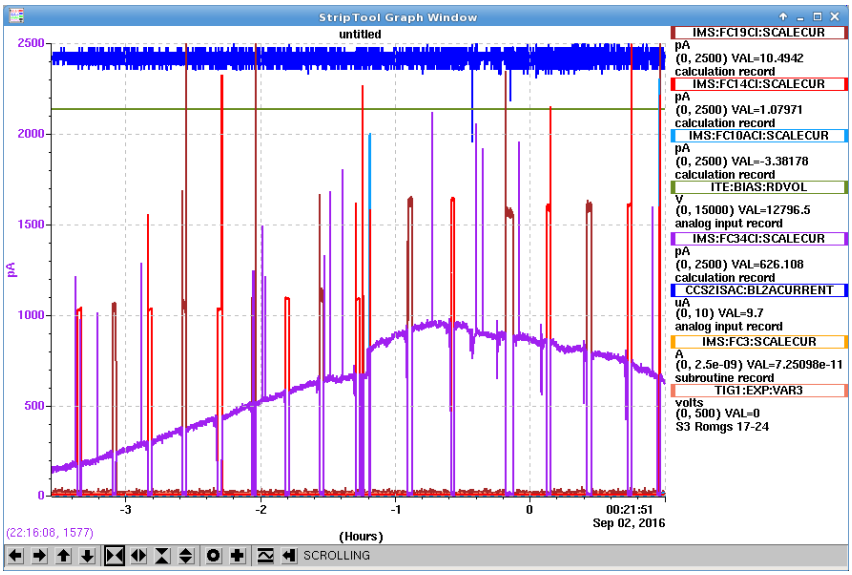

Figure 7: 238U FC34 Trend in purple.

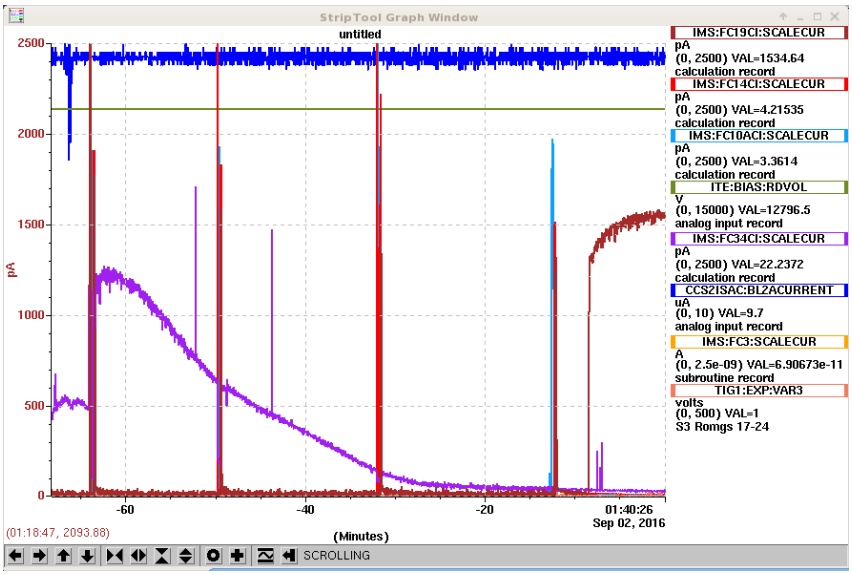

Figure 8: 94Sr FC34 Trend in purple.

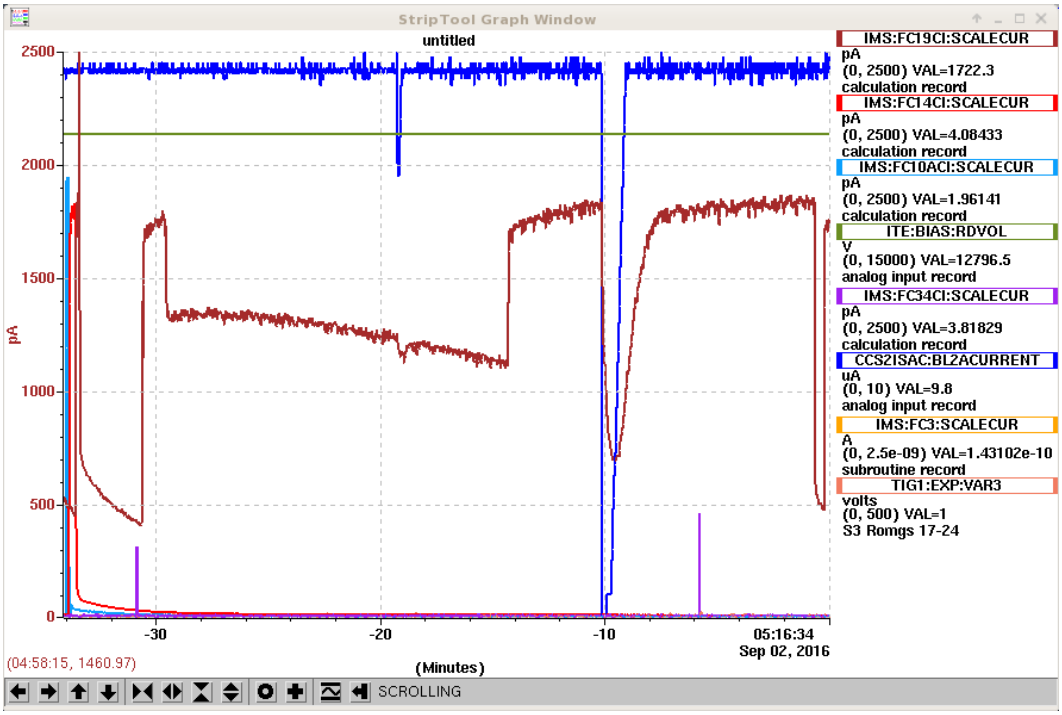

Figure 9: 94Sr FC19 Trend in brown.

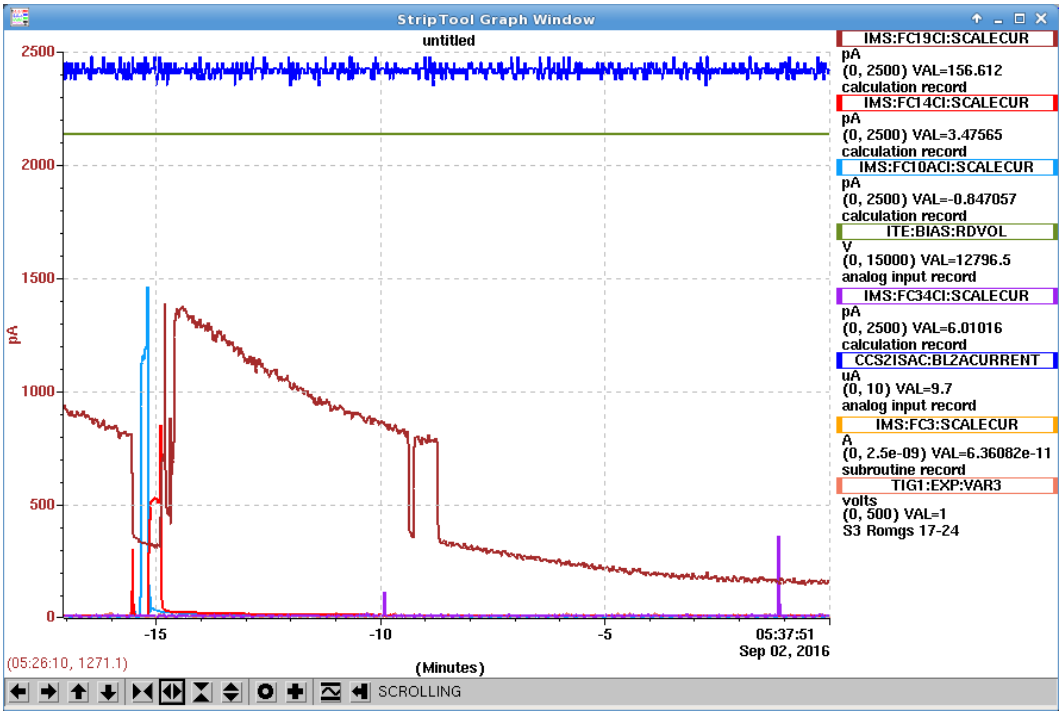

Figure 10: 94Sr FC19 Trend in brown.

3.2 Beam Position Evolution: 238U

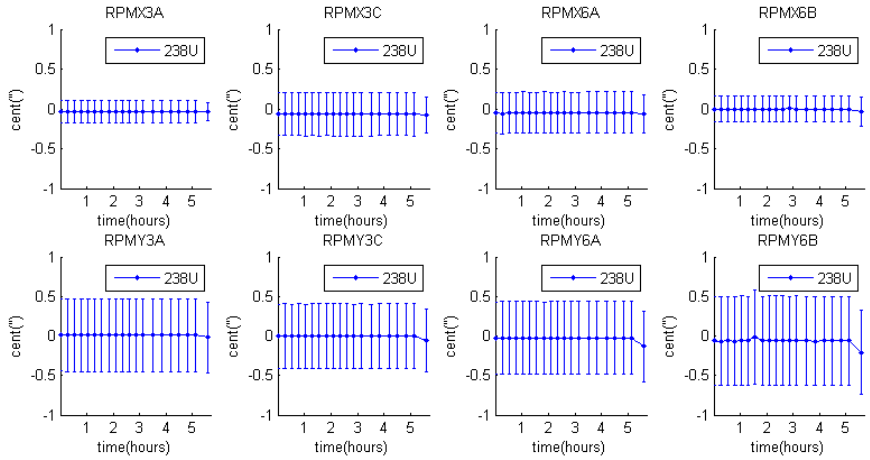

Figure 11: Run1: RPMs: 3A, 3C, 6A, and 6B. X_{cen} vs $t_{elapsed}$ Vertical centroid and rms in first row. Y_{cen} vs $t_{elapsed}$ Horizontal centroid and rms in second row.

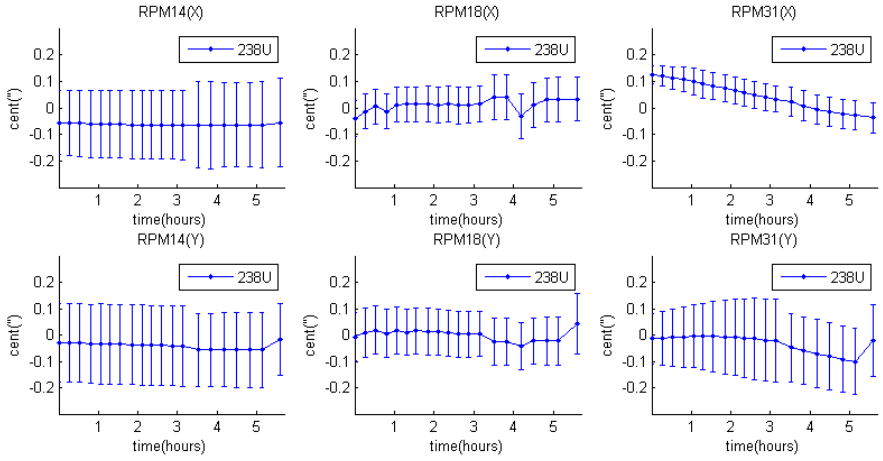

Figure 12: Run1: RPMs: 14, 18, 31. X_{cen} vs $t_{elapsed}$ Vertical centroid and rms in first row. Y_{cen} vs $t_{elapsed}$ Horizontal centroid and rms in second row.

3.3 Beam Position Evolution: 94Sr

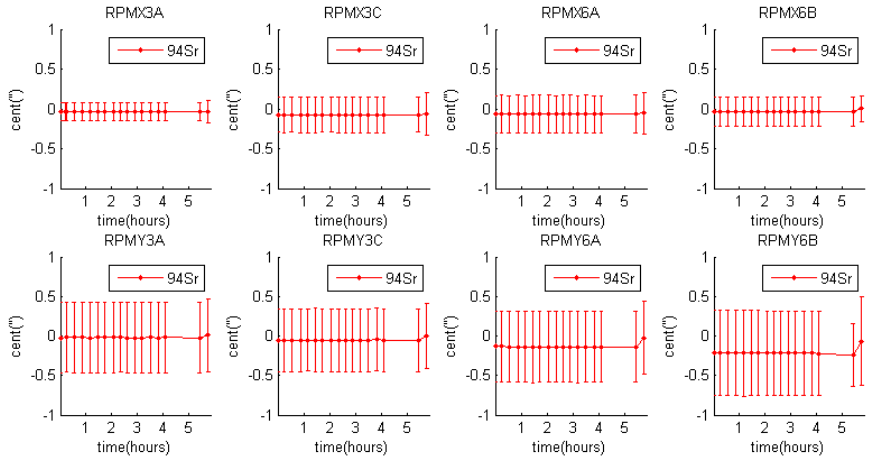

Figure 13: Run1: RPMs: 3A, 3C, 6A, and 6B. X_{cen} vs $t_{elapsed}$ Vertical centroid and rms in first row. Y_{cen} vs $t_{elapsed}$ Horizontal centroid and rms in second row.

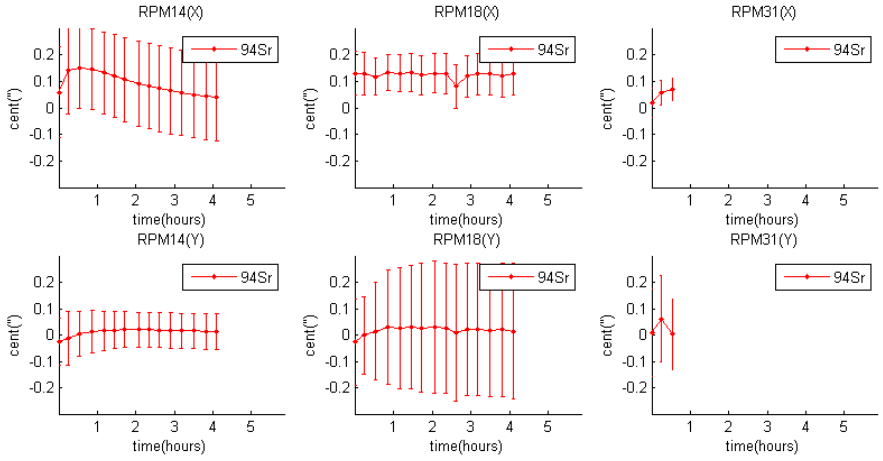

Figure 14: Run1: RPMs: 14, 18, 31. X_{cen} vs $t_{elapsed}$ Vertical centroid and rms in first row. Y_{cen} vs $t_{elapsed}$ Horizontal centroid and rms in second row.

3.4 Beam Position Evolution: RPM14 and RPM31

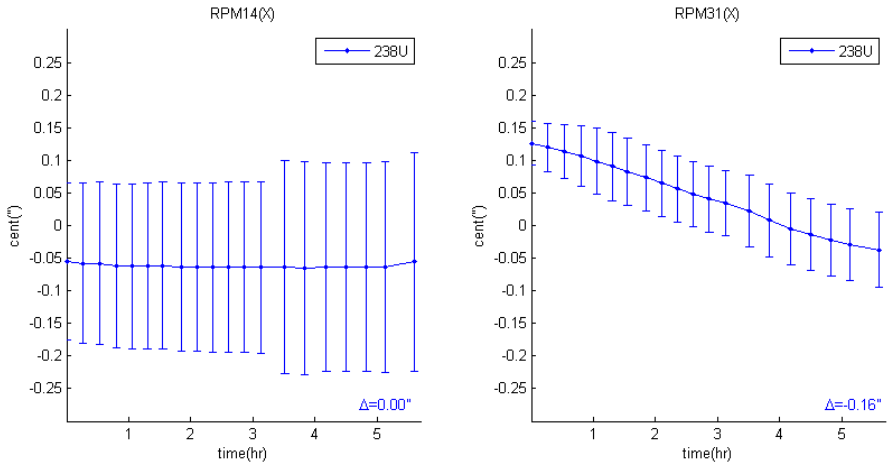

Figure 15: Run1: 238U X_{cen} vs $t_{elapsed}$. Vertical beam at RPM14 and RPM31. Error bars are profile scan RMS beam size, not an indication of measurement precision. At RPM31 the 238U beam is recovering its stable centerd position.

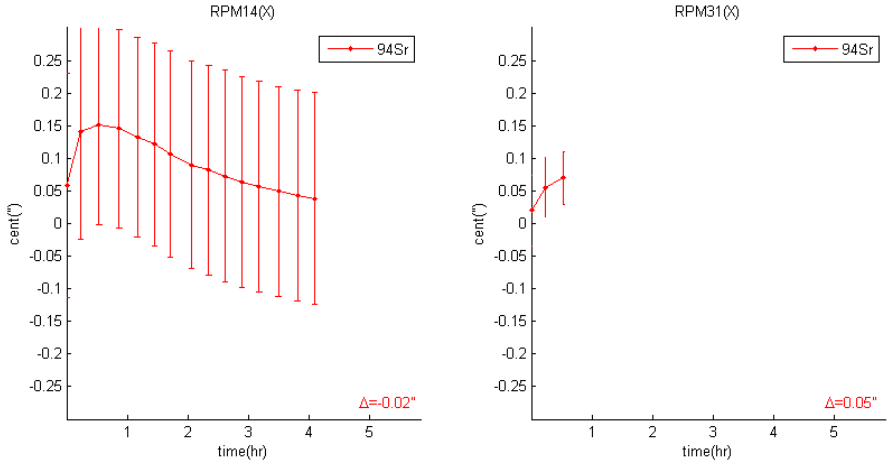

Figure 16: Run1: 94Sr X_{cen} vs $t_{elapsed}$. Vertical beam at RPM14 and RPM31. Error bars are profile scan RMS beam size, not an indication of measurement precision. The beam measurement data cannot be reconstructed at RPM31 within the first hour, and at RPM14 after four hours.

4 Run2: 2016/09/02 1hr 238U

4.1 Beam Position Evolution: 238U

Stable 238U beam for 1hr. Unfortunately no 94Sr data could be taken during this run (see Section 4.2).

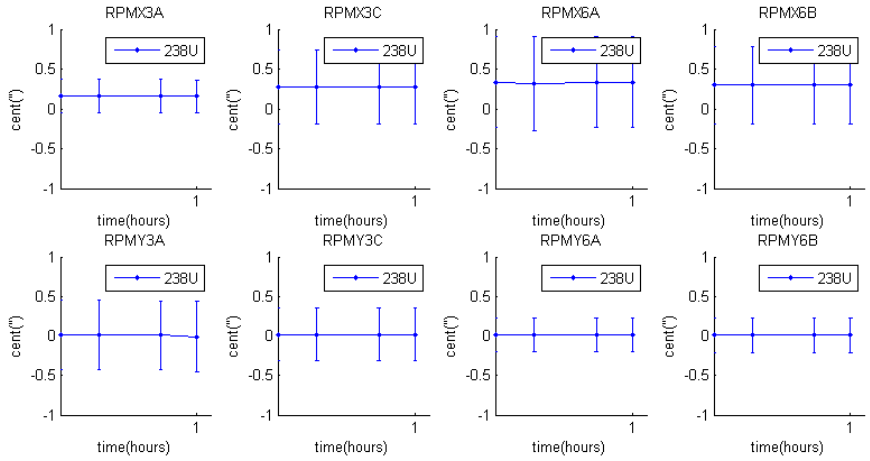

Figure 17: Run2: RPMs: 3A, 3C, 6A, and 6B. X_{cen} vs $t_{elapsed}$ Vertical centroid and rms in first row. Y_{cen} vs $t_{elapsed}$ Horizontal centroid and rms in second row.

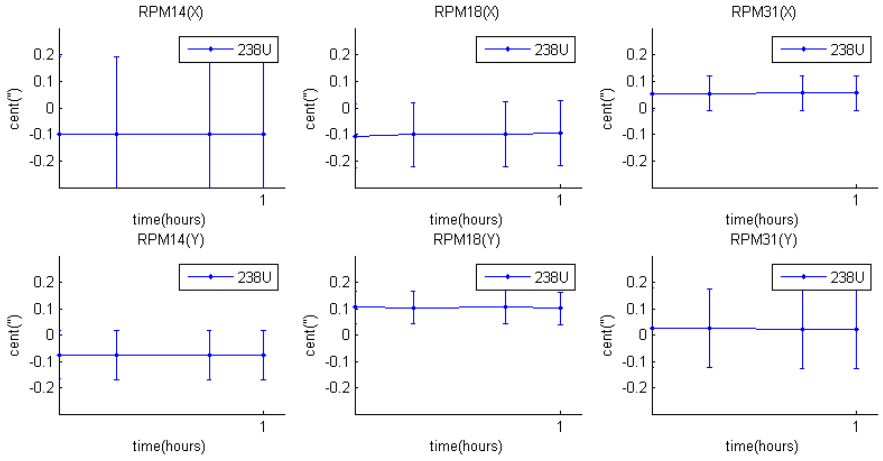

Figure 18: Run2: RPMs: 14, 18, 31. X_{cen} vs $t_{elapsed}$ Vertical centroid and rms in first row. Y_{cen} vs $t_{elapsed}$ Horizontal centroid and rms in second row.

4.2 Current Evolution

After one hour of stable 238U, the 94Sr beam is lost very quickly and no RPM data could be taken for 94Sr. Attempts to steer the beam upstream of FC34 were able to recover the current only temporarily.

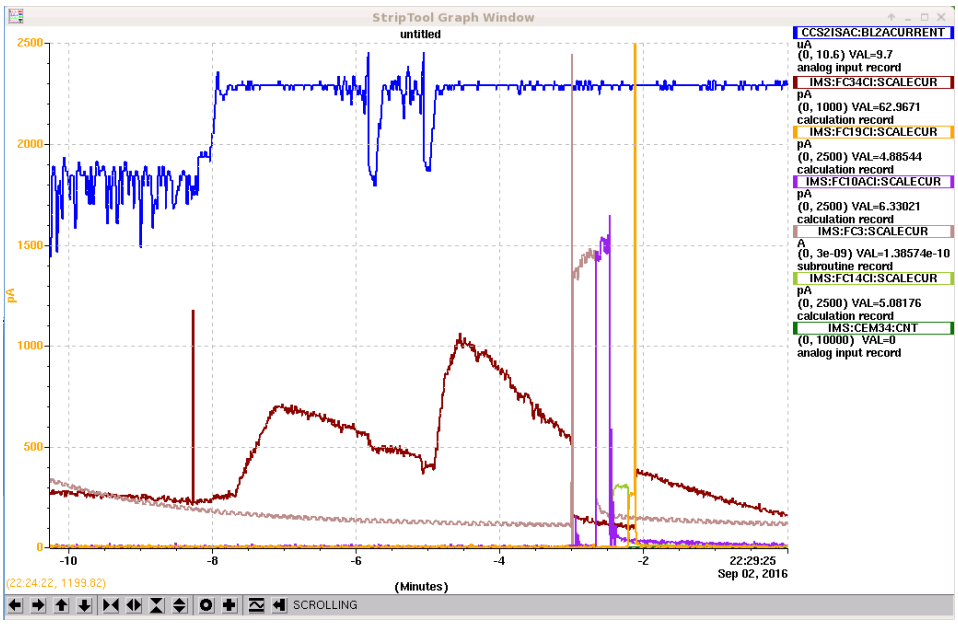

Figure 19: 94Sr FC34 Trend in brown.

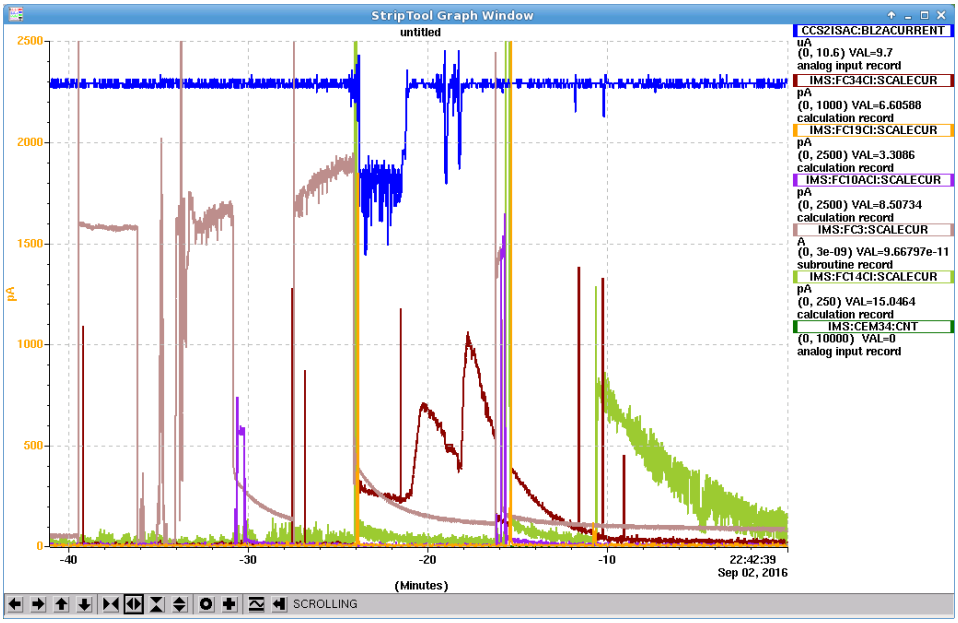

Figure 20: 94Sr FC34 Trend in brown, FC14 Trend in green.

5 Run3: 2016/09/03 3hr 238U → 2hr 94Sr

Run3 is characterized by a recovering 238U beam over 3 hours followed by steadily decreasing 94Sr current for two hours.

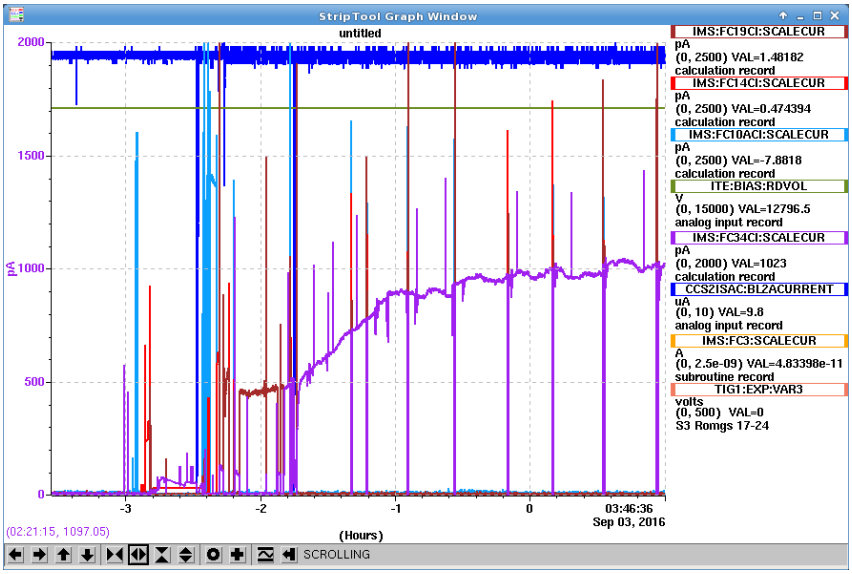

Figure 21: 238U FC34 Trend in purple.

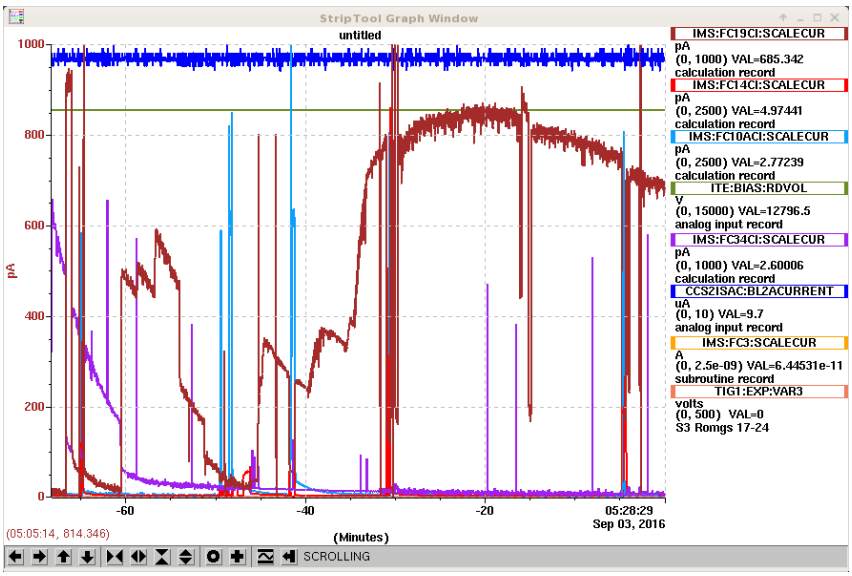

Figure 22: 94Sr FC19 Trend in brown.

5.1 Beam Position Evolution: 238U

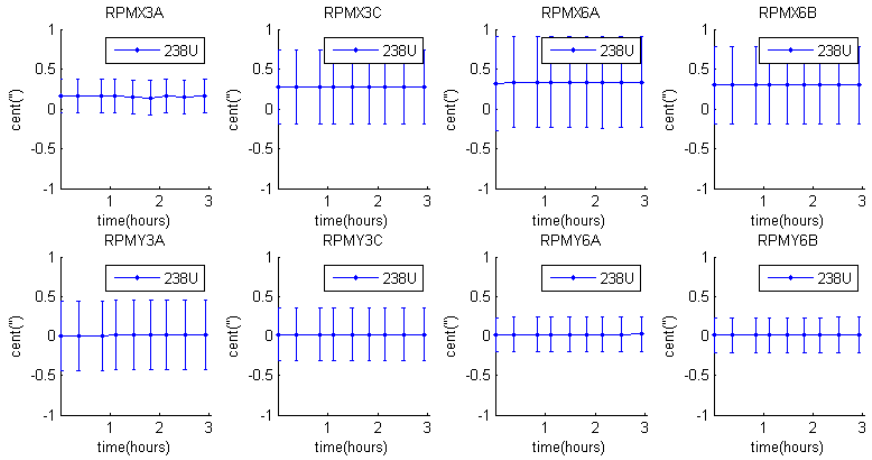

Figure 23: Run3: RPMs: 3A, 3C, 6A, and 6B. X_{cen} vs $t_{elapsed}$ Vertical centroid and rms in first row. Y_{cen} vs $t_{elapsed}$ Horizontal centroid and rms in second row.

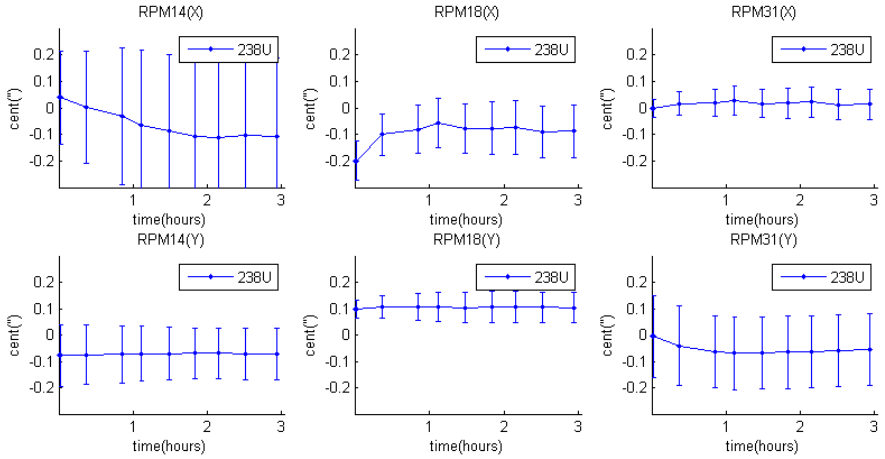

Figure 24: Run3: RPMs: 14, 18, 31. X_{cen} vs $t_{elapsed}$ Vertical centroid and rms in first row. Y_{cen} vs $t_{elapsed}$ Horizontal centroid and rms in second row.

5.2 Beam Position Evolution: 94Sr

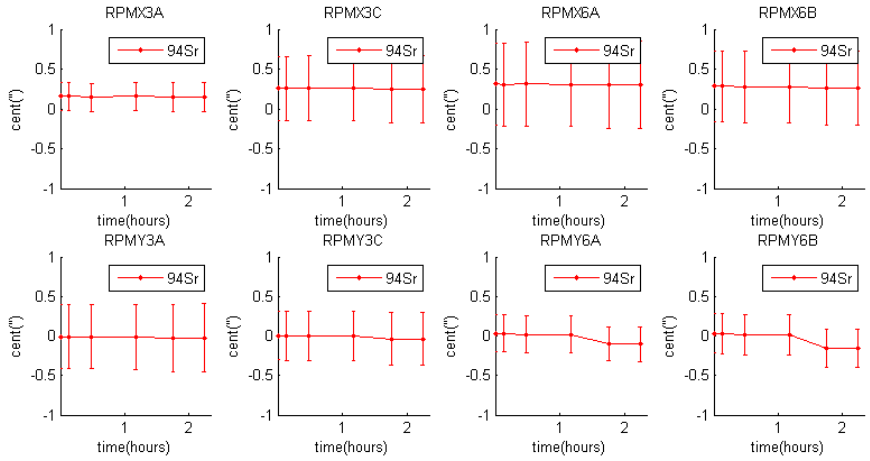

Figure 25: Run3: RPMs: 3A, 3C, 6A, and 6B. X_{cen} vs $t_{elapsed}$ Vertical centroid and rms in first row. Y_{cen} vs $t_{elapsed}$ Horizontal centroid and rms in second row.

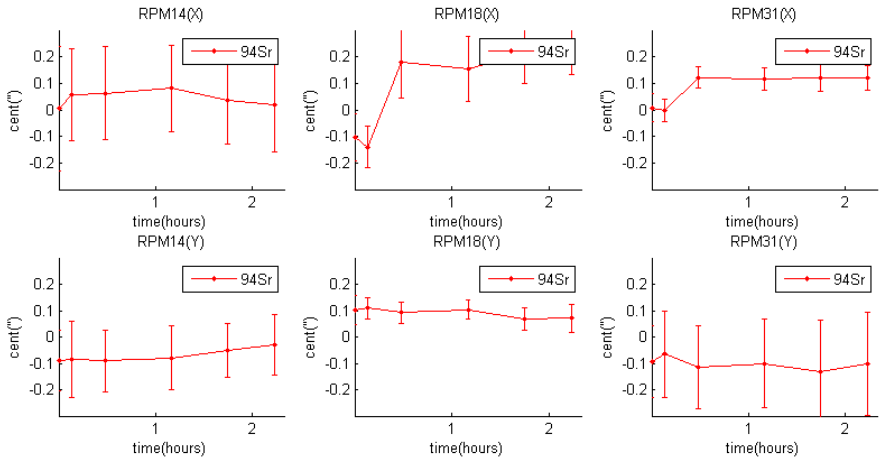

Figure 26: Run3: RPMs: 14, 18, 31. X_{cen} vs $t_{elapsed}$ Vertical centroid and rms in first row. Y_{cen} vs $t_{elapsed}$ Horizontal centroid and rms in second row.

5.3 Beam Position Evolution: RPM14 and RPM31

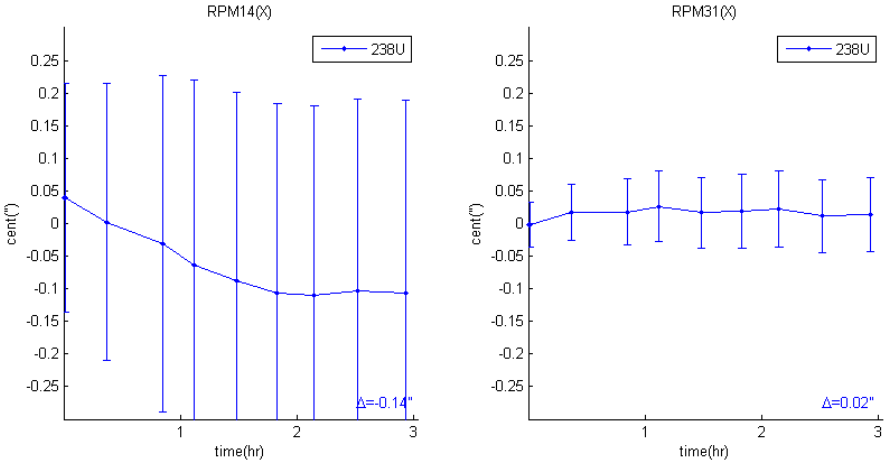

Figure 27: 238U.

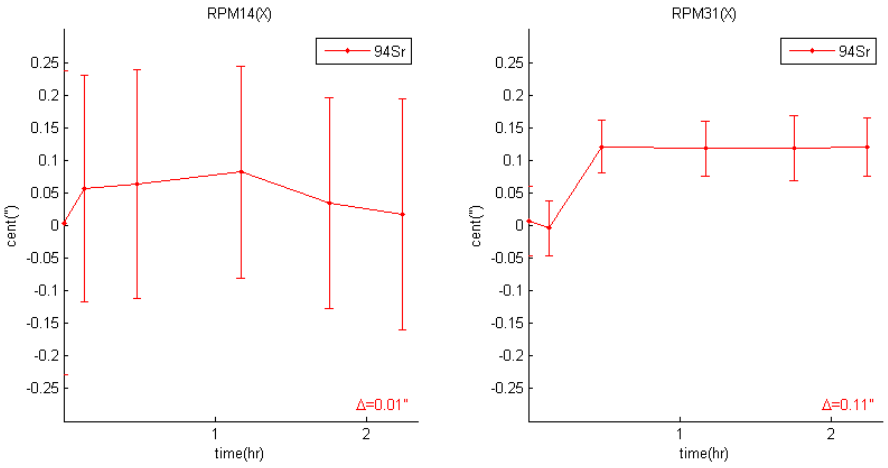

Figure 28: 94Sr.

6 Possible Causes

6.1 Charging Beamline Element

An element in the beamline (such as an electrode or slit plate) could have a poor grounding connection, and therefore errant beam particles might charge up this floating element which would induce steering on the beam.

6.1.1 Support

Steering the beam back recovers the current temporarily, so a charging element could be what is causing the beam to be deflected from its tune.

6.1.2 Conflict

At higher energies, it was thought that the beam's rigidity might mask this condition, meaning it would only be noticeable with low energy beams; however, the same effect was seen with 20kV and 28kV 94Sr beams.

This problem is also seen reliably with 94Sr beams, but not other species, which suggests that there is something chemistry-dependent going on.

6.2 Chemistry Considerations

Chemical compounds could potentially be forming on the surface of electrodes, and this coating could insulate the beam from the field produced by this electrode, effectively shielding the beam and needing to be compensated by increasing the steering.

β^- Process: A neutron spontaneously turns into a proton, an electron and an anti-electron neutrino. The daughter nucleus is often formed in an excited state and loses energy by gamma-ray emission. β^- decay occurs in nuclei on the neutron-rich side of the nuclear chart.[1]

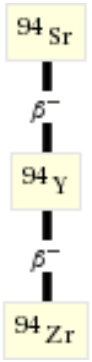

Figure 29: 94Sr Decay Chain.[3]

Authors: D. Abriola, A.A. Sonzogni Citation:Nuclear Data Sheets 107, 2423 (2006)

Parent Nucleus	Parent E(level)	Parent Jπ	Parent $T_{1/2}$	Decay Mode	GS-GS Q-value (keV)	Daughter Nucleus	Decay Scheme	ENSDF file
$^{94}_{38}Sr$	0.0	0+	75.3 s *2*	β^-: 100 %	3508 *8*	$^{94}_{39}Y$		

Beta-:

Energy (keV)	End-point energy (keV)	Intensity (%)	Dose (MeV/Bq-s)
171.1	538 *8*	0.080 % *20*	1.4E-4 *3*
412.1	1135 *8*	0.113 % *22*	4.7E-4 *9*
494.7	1326 *8*	0.76 % *11*	0.0038 *5*
831.3	2071 *8*	0.19 % *4*	0.0016 *3*
835.6	2080 *8*	98.1 % *9*	0.820 *8*
1506.9 ?	3508 *8*	0.5 % *5*	0.007 *7*

Mean beta- energy: 835 keV *13*, total beta- intensity: 99.7 % *10*, mean beta- dose: 0.832 MeV/Bq-s *16*

Figure 30: 94Sr.

Authors: D. Abriola, A.A. Sonzogni Citation:Nuclear Data Sheets 107, 2423 (2006)

Parent Nucleus	Parent E(level)	Parent Jπ	Parent $T_{1/2}$	Decay Mode	GS-GS Q-value (keV)	Daughter Nucleus	Decay Scheme	ENSDF file
$^{94}_{39}Y$	0.0	2-	18.7 m 1	β^-: 100 %	4918 7	$^{94}_{40}Zr$		

Beta-:

Energy (keV)	End-point energy (keV)	Intensity (%)	Dose (MeV/Bq-s)
70.5 ?	248 7	0.028 % 11	2.0E-5 8
80.7 ?	280 7	0.020 % 8	1.6E-5 6
224.8 ?	680 7	0.11 % 3	2.5E-4 6
240.0 ?	719 7	0.30 % 5	7.2E-4 12
279.9	820 7	0.022 % 12	6E-5 3
298.6	866 7	0.006 % 3	1.8E-5 9
319.2	916 7	0.011 % 6	3.5E-5 19
335.9 ?	956 7	0.27 % 4	9.1E-4 13
436.2 ?	1193 7	0.067 % 17	2.9E-4 7
596.1	1557 7	0.57 % 7	0.0034 4
659.8	1699 7	0.95 % 11	0.0063 7
732.5	1859 7	1.01 % 13	0.0074 10
801.9 ?	2010 7	0.21 % 4	0.0017 3
814.4	1973 7	0.078 % 18	6.4E-4 15
830.3	2072 7	0.41 % 5	0.0034 4
1053.7	2552 7	0.56 % 7	0.0059 7
1073.6	2586 7	0.015 % 15	1.6E-4 16
1154.6	2767 7	0.33 % 4	0.0038 5
1198.8	2860 7	5.3 % 5	0.064 6
1381.8	3247 7	3.3 % 4	0.046 6
1475.6	3448 7	4.1 % 4	0.060 6
1555.5	3618 7	1.83 % 20	0.028 3
1740.8	3999 7	39.6 % 22	0.69 4
2174.0	4918 7	41 % 4	0.89 9

Mean beta- energy: 1.81E+3 keV *13*, total beta- intensity: 100 % *5*, mean beta- dose: 1.81 MeV/Bq-s *15*

Figure 31: 94Y.

Element	Spectral Line	Formula	Energy (eV)
Al	2p	AlNiZr	71.80
Al	2p	AlNiZrOx	74.50
Al	2p	O2/AlNiZr	74.20
Al	2p	O2/AlNiZr	72.00
Al	2p	Zr[Al1.0O0.3(OH)0.8F1.0(H2O)0.7](C3H9N)1.3H0.3(PO4)2.2.3H2O	73.80
Al	2p	Zr[Al2.0O0.6(OH)1.4F2.3(H2O)1.4](C3H9N)0.7H0.5PO4)2.2.0H2O	73.70
Al	2p	Zr[Al3.4O1.1(OH)1.5F4.9(H2O)2.5](C3H9N)0.3H0.3PO4)2.2.9H2O	73.80
O	1s	Zr[Al3.4O1.1(OH)1.5F4.9(H2O)2.5](C3H9N)0.3H0.3PO4)2.2.9H2O	530.90
O	1s	ZrO0.15H2.25Na0.08[(AlO2)2.63(SiO2)93.37]	532.70
O	1s	Zr[Al2.0O0.6(OH)1.4F2.3(H2O)1.4](C3H9N)0.7H0.5PO4)2.2.0H2O	531.00
O	1s	Zr[Al1.0O0.3(OH)0.8F1.0(H2O)0.7](C3H9N)1.3H0.3(PO4)2.2.3H2O	531.00
P	2p	Zr[Al1.0O0.3(OH)0.8F1.0(H2O)0.7](C3H9N)1.3H0.3(PO4)2.2.3H2O	132.90
P	2p	Zr[Al2.0O0.6(OH)1.4F2.3(H2O)1.4](C3H9N)0.7H0.5PO4)2.2.0H2O	132.90
P	2p	Zr[Al3.4O1.1(OH)1.5F4.9(H2O)2.5](C3H9N)0.3H0.3PO4)2.2.9H2O	132.90
Si	2p	ZrO0.15H2.25Na0.08[(AlO2)2.63(SiO2)93.37]	102.90
Zr	3d5/2	ZrO0.15H2.25Na0.08[(AlO2)2.63(SiO2)93.37]	182.80
Zr	3d5/2	((ZrF4)53(BaF2)20(LaF3)4(AlF3)3(NaF)20)Ox	184.90
Zr	3d5/2	((ZrF4)53(BaF2)20(LaF3)4(AlF3)3(NaF)20)Ox	182.40
Zr	3d5/2	AlNiZr	179.00
Zr	3d5/2	Zr[Al3.4O1.1(OH)1.5F4.9(H2O)2.5](C3H9N)0.3H0.3PO4)2.2.9H2O	182.10
Zr	3d5/2	Zr[Al2.0O0.6(OH)1.4F2.3(H2O)1.4](C3H9N)0.7H0.5PO4)2.2.0H2O	182.10
Zr	3d5/2	(AlF3)4(BaF2)24(LaF3)4(NaF)15(ZrF4)53	184.60
Zr	3d3/2	(AlF3)4(BaF2)24(LaF3)4(NaF)15(ZrF4)53	186.90
Zr	3d5/2	Zr[Al1.0O0.3(OH)0.8F1.0(H2O)0.7](C3H9N)1.3H0.3(PO4)2.2.3H2O	182.10
Zr	3d5/2	O2/AlNiZr	182.50
Zr	3d5/2	O2/AlNiZr	179.00
Zr	3d5/2	AlNiZrOx	182.60

Figure 32: Al-Zr Compounds.[2]

Element	Spectral Line	Formula	Energy (eV)
Al	2p	O2/AlNiY	72.10
Al	2p	O2/AlNiY	74.20
Al	2p	AlNiYOx	73.80
Al	2p	AlNiY	72.00
Al	2p3/2	Y3Al5O12	73.17
Al	2p3/2	Y3Al5O12	74.00
Al	2p3/2	Y3Al5O12	73.77
Ca	2p3/2	(AlF3)0.40(YF3)0.16(BaF2)0.22(CaF2)0.22	348.29
Ca	2p3/2	(AlF3)0.40(YF3)0.16(BaF2)0.20(CaF2)0.22(BaCl2)0.02	348.29
Ca	2p3/2	(AlF3)0.40(YF3)0.16(BaF2)0.18(CaF2)0.22(BaCl2)0.04	348.29
Ca	2p3/2	(AlF3)0.40(YF3)0.16(BaF2)0.16(CaF2)0.22(BaCl2)0.06	348.29
Ca	2p3/2	(AlF3)0.40(YF3)0.16(BaF2)0.14(CaF2)0.22(BaCl2)0.08	348.29
Ca	2p3/2	(AlF3)0.40(YF3)0.16(BaF2)0.12(CaF2)0.22(BaCl2)0.10	348.29
Ca	2p3/2	(AlF3)0.40(YF3)0.16(BaF2)0.10(CaF2)0.22(BaCl2)0.12	348.29
Y	3d5/2	AlNiYOx	156.00
Y	3d5/2	O2/AlNiY	157.60
Y	3d5/2	O2/AlNiY	155.90
Y	3d5/2	AlNiY	155.60

Figure 33: Al-Y Compounds.[2]

6.2.1 Support

At 12.78kV if other mass beams are stable, this would indicate that possibly something specifically chemistry-dependent is occurring with 94Sr beams.

6.2.2 Conflict

Certain phenomena still need to be explained, such as reducing the slit aperture increasing the beam current downstream. Y half-life of 18.7m may be too long for Zr to have contributed meaningful to fast decline in current seen in Figures 19 and 20.

In Run0 (Section2.1), the current decreases at a steady rate over two hours. However, in Run2 (Section 4.2), the current decreased at a much faster rate over twenty minutes. Whichever process accounts for this beam loss would need to explain both time scales.

7 Conclusions

Stable beam centroids from RPM3A-RPM6B for all 94Sr runs indicate that the issue lies downstream of RPM6B. Small but consistent centroid deviations at RPM14 (with larger deviations at RPM31) indicate that the issue is introduced upstream of RPM14.

The position deviation seems to be in the vertical plane, but this is not conclusive. More systematic observations are needed to further narrow down the specific location of the problem, or determine if it is chemisty-dependent (downstream of the bending magnet may be an indication?).

In addition, there were three other runs not summarized in this note because of missing or untrusted data. In some cases, only screencaptures are available in the ISAC E-log (without raw data saved). In other cases, the raw data is available when it was saved as all RPM data together at a certain timestamp. However, the analyzed data for a given RPM sometimes ended up being exactly the same from one timestamp to another. In this case it can not be known definitively whether the beam has not moved, or if a new scan was not taken at that RPM.

Automatic saving of each RPM scan individually is therefore proposed to avoid loss of data in the future, and to ease the operators workload from having to save the data manually with timestamps. This will also prevent confusion when saving all RPM data together, as a timestamp could be available for each individual RPM scan (not just knowing that it was the last scan taken at that location). The mode of saving all RPM data together can still be employed for E-log entries, while the individual RPM data can facilitate beam studies. Communication with the controls group will be initiated to solve this issue.

Another problem encountered was the malperformance of diagnostic elements in the beamline. RPM22 and RPM24 were not providing reliable data, and it is seen that RPM18 may be slowly approaching this same unuseable state. Systematic studies to understand unknown beam behavior cannot be fully realized without the availability of all diagnostic elements in the immediate vicinity. It is important to therefore begin the process of having these RPMs replaced or repaired.

Summary: Snapshot ITE → IMS:FC19/34

	Run0	Run1
Beam	94Sr @ 12.78kV	94Sr @ 12.779kV
ITE Bias Voltage [V]	12796.5	12796.5
ITE Bias Current [uA]	83.9	84.2
ITE EE Voltage [V]	612.9	612.9
ITE EE Current [mA]	0.586	0.586
ITE EL Voltage [V]	5257.0	5257.0
ITE EL Current [uA]	19.1	19.1
Target Current [A]	360.00	360.00
Target Voltage [V]	4.70	4.69
Tube Current [A]	235.00	235.00
Tube Voltage [V]	3.28	3.28
p+ [uA]	9.7	9.7
Pre-Separator [G]	-2901.13	-2901.14
Separator [G]	-1483.42	-1483.45
Alpha [A]	0.35	0.35
Beta [A]	3.17	3.17
IMS:MB1 M/Q	93.8264	93.827
IMS:MB2 M/Q	94.0242	94.028
IMS:YSLIT0 width [mm]	2.00	2.00
IMS:YSLIT10A width [mm]	4.17	4.17
IMS:YSLIT10A position [mm]	31.75	31.75
IMS:YSLIT11 width [mm]	2.80	2.80
IMS:YSLIT22 width [mm]	20.00	20.00
IMS:XSLIT22 width [mm]	20.00	20.00
IMS:YSLIT24 width [mm]	18.53	18.53
IMS:XSLIT24 width [mm]	20.00	20.00
IMS:ATT18	Out	Out

References

[1] http://www.triumf.ca/radioactive-decay-modes

[2] http://www.nndc.bnl.gov/nudat2

[3] http://www.wolframalpha.com